# A Study of Photocatalytic Degradation of Dyeing and Printing Wastewater by ZnO@zeolitic Imidazolate Framework (ZIF)-8

**MU HONGJUN[1, 2], DING SHAOLAN[1] and DENG LANG[2]**

*[1] College of Bioresources Chemical and Materials Engineering, Shaanxi University of Science & Technology*

*[2] School of Light Industry and Engineering, Qilu University of Technology*

**Abstract**

As a semiconducting material with outstanding properties, ZnO has been playing a key role in the chemical industry, light industry, ceramics, electronics, national defence, healthcare and other high-tech industries. In recent years, great efforts have been made in studies of ZnO as photocatalyst in the treatment of organic wastewater by virtue of its high reaction rate, excellent applicability and environmentally friendly products. The metal-organic frameworks (MOFs) exhibit large specific surface area and good stability, and calcination of zeolitic imidazolate framework (ZIF)-8 in atmosphere leads to generation of ZnO@MOF. With relatively large specific surface areas, ZnO nanoparticles can generate a large quantity of hydroxyl free radicals under visible light and these radicals can non-selectively oxidise most organics (strong organic-oxidising capability). ZIF-8 was synthesised using the hydrothermal method and calcinated at different temperatures to obtain ZnO nanoparticles of different sizes. Then, the photocatalytic performances of these ZnO nanoparticles were tested by degradation of methylene blue (MB) under visible light. Additionally, the ZnO samples were applied in photocatalytic degradation of dyeing and printing wastewater produced by leather retanning. The chemical oxygen demand (COD) removal rate and the total organic carbon (TOC) mineralisation rate exceeded 70% and 35%, respectively.

Tannery wastewater refers to the industrial wastewater discharged by tannery yards. It contains considerable organics and non-degradable dyes, which increase the oxygen consumption of water. Indeed, organics and non-degradable dyes are severe environmental hazards as their treatments (to meet the emission standards) are extremely challenging. Current treatment methods include physicochemical treatment, biochemical treatment and combined method. However, these methods have their respective limitations in treatment of organic pollutants. Recently, studies of semiconductors as photocatalysts for degradation of various pollutants have attracted great attention both in China and globally.[1,2]

As a novel nanomaterial, metal-organic frameworks (MOF) are characterised by large specific surface area, adjustable rich porosity, high density of active sites. As a key N-type semiconductor, ZnO has been widely applied in various areas, including environmental protection, optics, electrics and catalysis.[3-9] With a bandgap of 3.2eV, ZnO can only absorb UV light (with wavelength below 380 nm) in theory, while absorbance of visible light by ZnO is supposed to be extremely low.[10] Hence, catalytic oxidising degradations of wastewater with ZnO as photocatalyst shall be under UV light, which limits their industrial applications. To enhance the photocatalytic performance of ZnO under visible light, researchers have tried several methods, including noble metal deposition, semiconductor composition, non-metallic doping, metal ion doping and carbon loading.[11-18]

In this study, ZIF-8 (precursor) was synthesised using a hydrothermal method and calcined at different temperatures to obtain ZnO nanoparticles with different sizes. Characterisation by XRD, SEM, TEM and EPR revealed that calcined ZnO samples have large specific surface areas and rich porosity. The photocatalytic performances of different ZnO nanoparticles were evaluated by degradation of methylene blue (MB) under visible light to investigate the effects of morphology, crystal face, surface free radicals, pH and particle size of the ZnO and illumination time on their photocatalytic performances. Additionally, ZnO was employed as a photocatalyst in degradation of dyeing and printing wastewater produced by leather retanning under visible light, and the chemical oxygen demand (COD) removal rates and the total organic carbon (TOC) mineralisation rates were calculated.

## 1 EXPERIMENTAL PROCEDURES

### 1.1 Agents

Zinc nitrate hexahydrate (AR) was purchased from Aladdin (Shanghai); 2-methylimidazole (AR) was purchased from Sigma-Aldrich (China); ammonia (AR) and methanol (AR) were purchased from Shanghai Lingfeng Chemical Reagent Co., Ltd.; MB (AR) was purchased from the Tianjin Institute of Chemical Reagents.

### 1.2 Synthesis of ZnO@ZIF-8 and ZnO@MOF

According to previous reports 19-23, $Zn(NO_3)$•$6H_2O$ and 2-methylimidazole were dissolved in methanol solution in a mass ratio of 1:2.5. Specifically, zinc nitrate was added into 2-methylimidazole solution dropwise under fierce stirring and then stirred at room temperature for 24 hours. The white precipitate was filtered, rinsed repeatedly by methanol, and dried at 80°C for 24 hours to obtain ZIF-8 samples. The obtained ZIF-8 samples were placed in a tube furnace

and heated in the atmosphere at 2°C/min. The samples were calcined at 400°C, 500°C, 600°C, 700°C, and 800°C, respectively, for 3 hours, followed by natural cooling to room temperature. The ZnO powders were labelled as Z400, Z500, Z600, Z700, and Z800, accordingly.

### 1.3 Characterisation

ZnO@ZIF-8 was calcined to obtain ZnO@MOF, whose morphology and structure were checked by X-ray diffraction (XRD, Miniflex 600), scanning electron microscope (SEM, Hitachi S-4800), transmission electron microscope (TEM, JEM-2010), DTA-thermogravimetric analyzer (DTA-TGA, 49F), electron paramagnetic resonance (EPR, AVANCE II 400).

### 1.4 Photocatalysis tests

*1.4.1 Photocatalytic degradation of methylene blue (MB)*

50mg of the prepared samples and a commercially available ZnO were added into 50mL $10^{-5}$mg/L MB solution and sonicated for 15 minutes at room temperature. The suspension was placed in a photochemical reactor and stirred in the dark for 30 minutes to achieve adsorption/desorption equilibrium of organic pollutants and photocatalyst. A 5mL sample was collected and centrifuged for 10 minutes. The suspension containing photocatalyst and organic pollutants was stirred at 460 r/min under xenon lamp. A sample was collected every 30 minutes and centrifuged at 5000r/min for 10 minutes. The absorbance of supernatant was checked by UV-5500 spectrophotometer. As the absorbance of suspension is proportional to its concentration at relatively low concentrations, the photocatalytic degradation rate of MB can be denoted as:

$$(A_0\text{-}A_t)/A_0$$

Where: $A_t$ refers to absorbance of the sample after t; $A_0$ refers to absorbance of initial MB solution.

Additionally, the photocatalytic performances of Z400, Z500, Z600, Z700, and Z800 in MB solutions with different pH values (3, 5, 7, 9, 11 and 13) were investigated by the proposed approach.

*1.4.2 Photocatalytic degradation of tannery wastewater*

The procedures of photocatalytic degradation of tannery wastewater were consistent with those of photocatalytic degradation of MB. The photocatalysis efficiency was evaluated by measuring wastewater COD removal rate and TOC mineralisation rate before and after photocatalytic degradation.

$$\text{COD removal rate } Y_{COD} = (C_0\text{-}C_t)/C_0$$
$$\text{TOC mineralisation rate } Y_{TOC} = (T_0\text{-}T_t)/T_0$$

## 2 RESULTS AND DISCUSSION

### 2.1 Structure and morphology of ZnO@ZIF-8

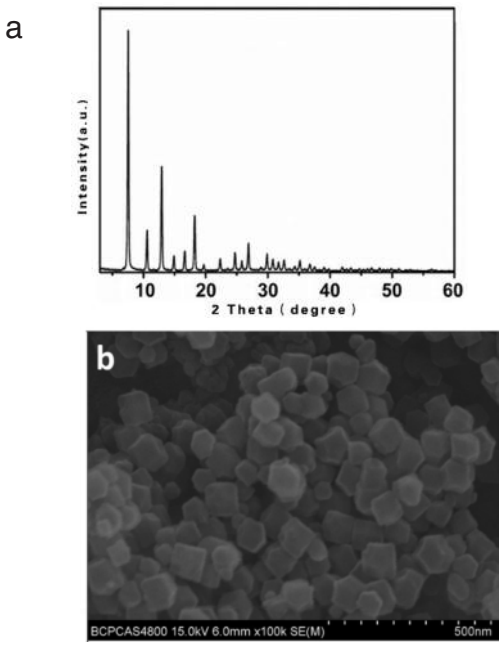


**Figure 1**. XRD (**a**) and SEM (**b**) of ZIF-8 samples.

Figure 1 shows the XRD and SEM images of ZIF-8 sample, which are consistent with those reported elsewhere. As observed, the ZIF-8 crystals are in a regular octahedron structure.

### 2.2 TG analysis of ZnO@ZIF-8

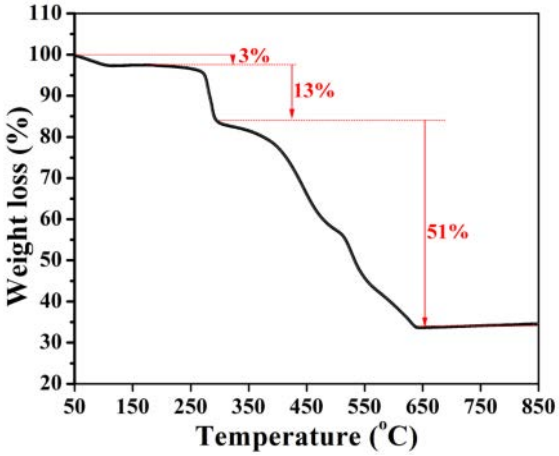


**Figure 2**. Thermogravimetric curve of ZIF-8.

As shown in Fig. 2, 3% and 13% weight losses were observed at 100°C and 280°C, respectively. At 300-600°C, structural changes were observed and the weight loss of organic ligands was 51% at 600°C, accompanied by structural collapse. After 600°C, thermal weight loss remained at 33%.

### 2.3 Structure and morphology of Z400, Z500, Z600, Z700, Z800

Figure 3 shows the XRD pattern of a ZIF-8 sample. It can be seen from the figure that the sample has a good crystallinity. The spectrum corresponds to the PDF standard card (JCPDS no.36-1451).

As shown in Fig. 4 (a-c), SEM of Z400, Z500 and Z600 prepared at different calcination temperatures

show that ZnO particles become finer and more regular with the increase of temperature. The higher the temperature is, the finer the particles are. Figure 4 (d) shows the TEM of Z600, which has nanostructure. In Fig. 4 (e), clear lattice striations are seen and the (001) crystal surface is exposed, with a d of 0.29nm. Figure 4 (f) shows the diffraction aperture of ZnO crystal.

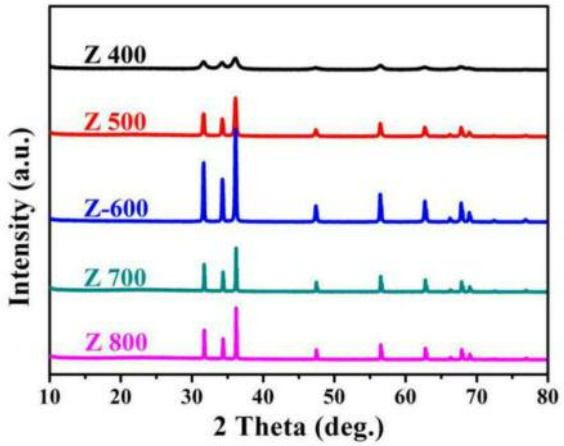


**Figure 3.** X-ray diffraction patterns of Z400-Z800.

Z700 and Z800 in Fig. 5 are ZIF-8 samples calcined at 700°C and 800°C. As observed, surface carbonisation and structural collapse were observed, and morphologies of these samples were not as regular as that of Z600, although the nano-structure was maintained. As shown in Fig. 5(a) a structure collapse occurred in TEM of Z700 compared with Z600.

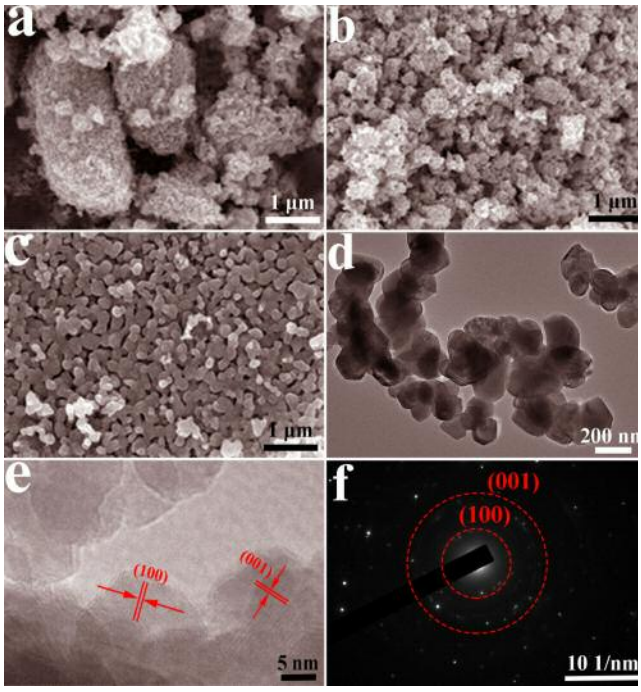


**Figure 4**. (**a-c**) SEM of Z400, Z500, Z600, TEM of (**d**) Z600, (**e**) lattice fringe, (**f**) crystal diffraction ring.

### 2.4 EDS of Z400, Z500, Z600

As shown in Fig. 7 a, b and c, the carbon content decreased as the calcination temperature increased. Indeed, the carbon contents of Z400 and Z500 were

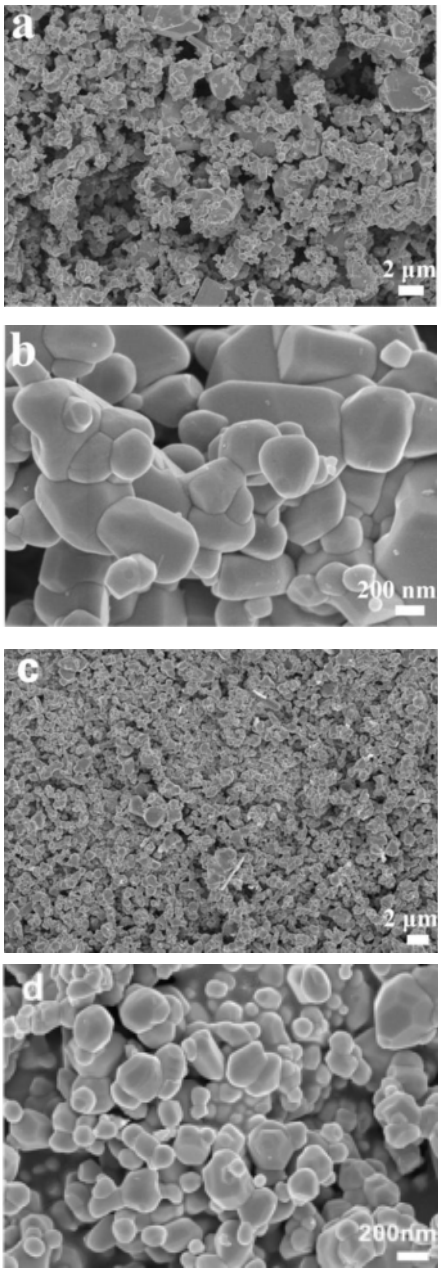


**Figure 5**. (**a-b**) SEM of Z700, (**c-d**) SEM of Z800

60%, while that of Z600 was 20%; the zinc contents of Z400 and Z500 were 20%, while that of Z600 was 70%.

### 2.5 EPR results of Z400, Z500, Z600

The g factor was calculated (by g=hv/flH) to be 2.006. Meanwhile, a comparison of slopes revealed that EPR curves of the four samples were all Gaussian. This can be attributed to resonance of various paramagnetic particles in different magnetic fields. Compared with other samples, Z600 are characterised by a large quantity of oxygen vacancies, resulting in high density of active sites, which effectively prevent recombination of photogenerated carriers.

### 2.6 Photocatalytic performances of ZnO (calcined at different temperatures) in photocatalytic degradation of MB

Figure 8 shows the trends of MB degradation rates by different samples. Under illumination by visible light,

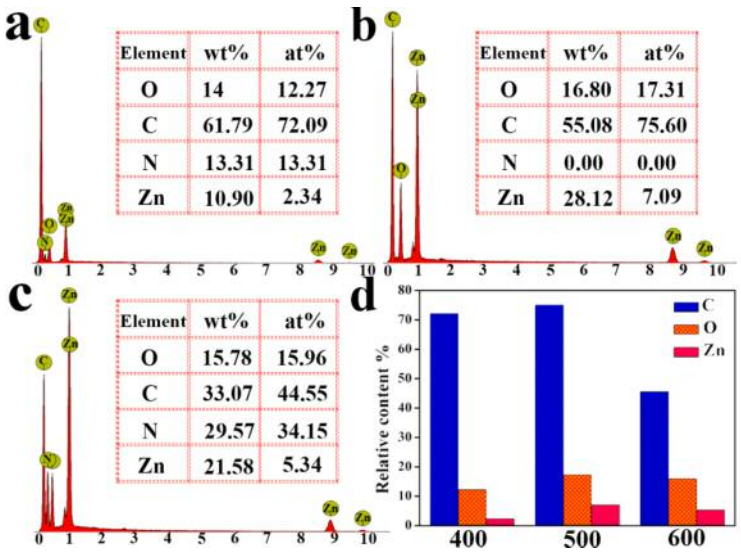


**Figure 6**. (**a-c**) shows EDS element analysis in Z400,Z500 and Z600, and (**d**) shows the relative content of each element

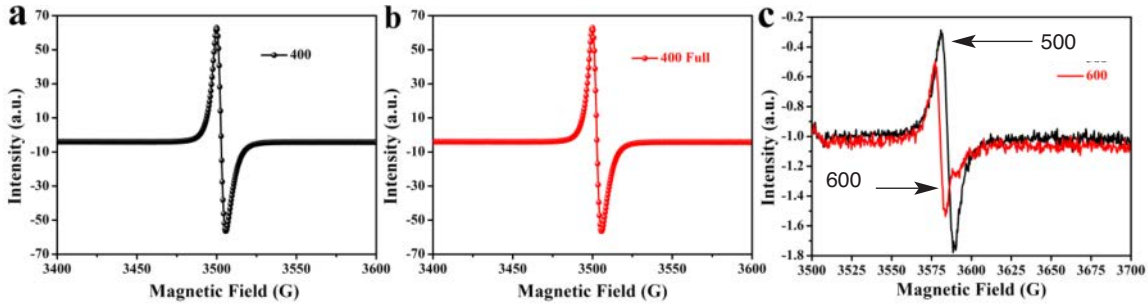


**Figure 7**. EPR spectra (**a**) is Z400, (**b**) is commercial ZnO and (**c**) is Z500 and Z600.

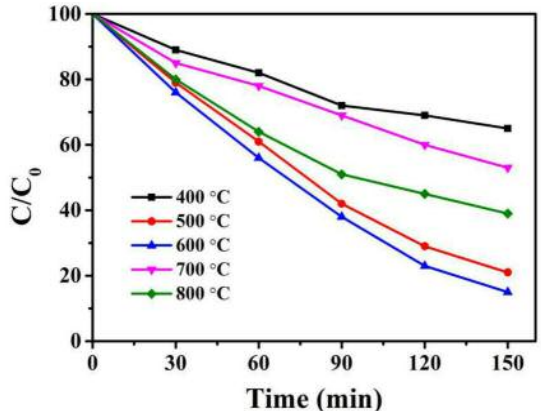


**Figure 8**. $C/C_0$ curve of photocatalytic degradation of MB by ZnO prepared at different calcination temperatures over time.

degradation rates of MB catalysed by Z400, Z500 and Z600 were 33%, 77.29%, and 82%, respectively. Indeed, the degradation rate of MB catalysed by Z600 was higher than those by Z400 and Z500, while degradation rates of MB catalysed by Z700 and Z800 were lower than that by Z500. This can be attributed to the collapses of ZIF frameworks in Z600, Z700 and Z800, which hinders exposure of active sites of metallic ions, thus preventing redox reactions of dye molecules with these active sites, resulting in reduced degradation rate of MB. Therefore, Z600 exhibited optimised photocatalytic performance among all samples involved.

### 2.7 Effects of pH on photocatalytic performance of ZnO

As shown in Fig. 9, the photocatalytic performance was positively related to the pH value. At pH13, the photocatalytic performance was optimised: the degradation rates of MB catalyzed by Z400, Z500 and Z600 were 60%, 98.88% and 89.83%, respectively. The UV-Vis spectra of MB solutions after photocatalytic degradation by ZnO@MOF were consistent with this conclusion. Among the three ZnO samples, Z500 exhibited highest catalytic rate. Indeed, the degradation rate by Z500 at 30 min was 90%, which was achieved by Z600 at 60 minutes.

### 2.7 Photocatalytic degradation of tannery dyeing wastewater by Z400-Z800

Figures 10 and 11 illustrate the TOC and COD values of tannery wastewater samples before and after visible light photocatalysis by Z400-Z800, respectively. CODs were measured using the bichromate method. As observed, Z600 exhibited optimised performance as photocatalyst in degradation of tannery dyeing wastewater, with COD removal rate ($Y_{COD}$) of 82% and mineralisation rate ($Y_{TOC}$) of 33%.

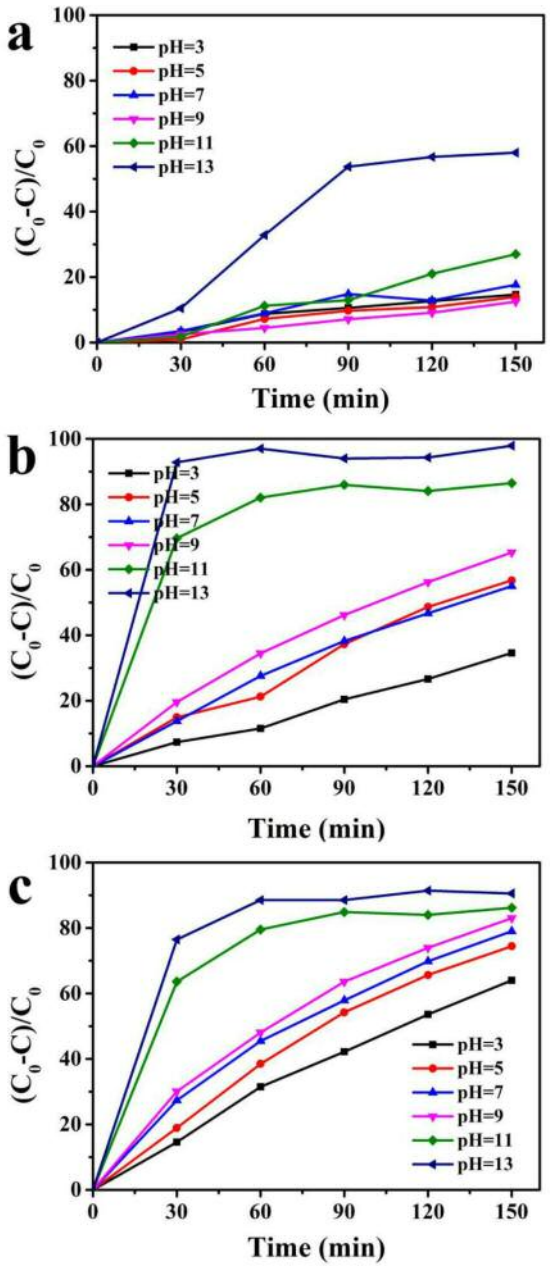


**Figure 9**. Degradation rates of Z400, Z500 and Z600 for photocatalytic degradation of MB over time under different pH conditions.

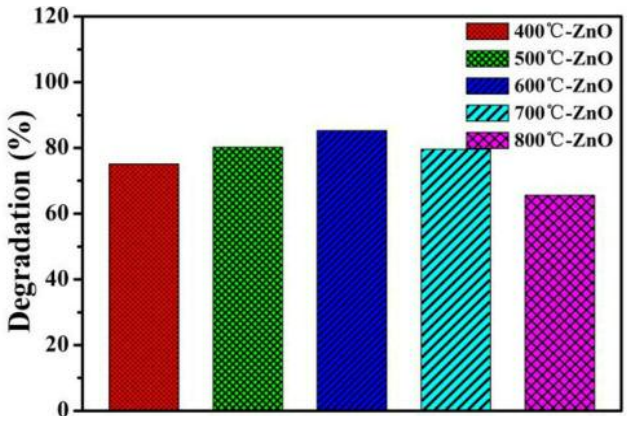


**Figure 10**. COD removal rate of dyeing wastewater degraded by Z400-Z800.

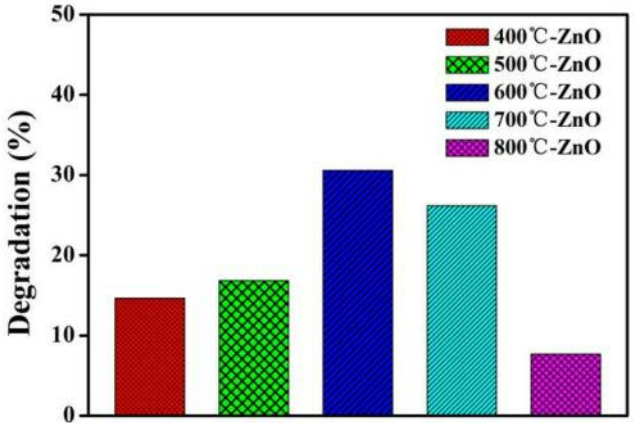


**Figure 11**. Z400-Z800 degradation of dyeing wastewater TOC mineralisation rate.

## 3. CONCLUSIONS

ZnO@ZIF-8 was synthesised using hydrothermal method and calcined at 400, 500, 600, 700 and 800°C, respectively, to obtain ZnO nanoparticles of different sizes (Z400, Z500, Z600, Z700, Z800). According to the TGA curves, frames of ZnO collapsed upon calcination at temperatures above 600°C. The activity of a photocatalyst is determined by the density of hydroxyl free radicals generated and crystal faces with high activation energy facilitate generation of oxygen free radicals. Hence, exposure of crystal faces with high activation energy shall be optimised during synthesis of ZnO samples. The photocatalytic performances of prepared ZnO nanoparticles were evaluated by using them as photocatalysts in visible light photocatalysis of MB. The degradation rate of methylene blue (MB) catalyzed by Z600 reached 90%. The degradation rates of MB catalyzed by all ZnO samples were proportional to the pH value. At pH13, degradation rates of MB catalyzed by Z400, Z500, Z600 exceeded 98%, if not reaching 100%. Additionally, COD removal rate and TOC mineralisation rate of degradation of tannery wastewater by prepared samples exceeded 80% and 33%, respectively. This can be attributed to the relatively large specific surface areas of nano-semiconducting ZnO nanoparticles. Owing to the large specific surface areas, considerable numbers of hydroxyl free radicals were generated under visible light and these radicals are responsible for catalytic oxidation of dye molecules. As the calcination temperature increased, ZnO nanoparticle size decreased, and the specific surface area increased. As a result, current-carrying electrons and holes reached the crystal faces faster and the probability of electron-hole recombination dropped, resulting in enhanced photocatalysis efficiency.

*(Received May 2019)*

*in association with China Leather*

**References**


1. Chong, M. N., Jin, B., Chow, C. W. *et al.,* Recent developments in photocatalytic water treatment technology: A review. *Water Research*, 2010, **44**(10), 2997
2. Huang Bing-hua, Zhang Xiao-fei, Song Lei *et al.,* Overview of $TiO_2$ photocatalytic water treatment technology. *Water Treatment Technology*, 2014, **40**(3), 11.
3. Murnganandham, M., Chen, I. S. and Wu, J., Effect of temperature on the formation of macroporous ZnO bundles and its application in photo catalysis. *J. Hazard. Mater.,* 2009, **172**(2), 700.
4. Kong, X. R., Liu, I., Qiu, C. *et al.,* Research progress of ZnO nanorod. *J. Materials Review,* 2009, **23**(3), 105.
5. Xu, X. N., Zhang, Q. P. *et al.,* Effects of different calcination temperatures on photocatalytic effects of nano-ZnO in sol-gel synthesis. *Materials Review B: Research,* 2016, **30**(1), 18.
6. Song Younan, Preparation of modified ZnO photochemical agent and its photocatalytic degradation of antibiotic wastewater. Master's thesis of Chang 'An University. 2013: 20-23.
7. Liu Bingbing, Preparation of ZnO materials with different morphologies and their photocatalytic properties. Master's thesis of Henan University, 2014: 11-43.
8. Li Yao, Xie Zongxian and Chen Haixin, Preparation and photocatalytic properties of isonitrogen-doped ZnO tetrapod. *J. Dongguan Institute of Technology*, 2016, **23**(5), 63.
9. Huang Xinyou, Deng Yuehuan, Li Xiaoyi *et al.,* Effects of three modification methods on photocatalytic properties of nanometer ZnO catalyst powders. *School of Artificial Products*, 2012, **41**(3), 718.
10. Behnajady, M. A., Modirshahla, N., Daneshvar, N. *et al.,* Photocatalytic degradation of CI Acid Red 27 by immobilized ZnO on glass plates in continuous mode. *J. Hazard. Mats.,* 2007, **140**(1), 257.
11. Liu, G., Chen, H., Chakka, L. *et al.,* Further search for selectivity of positron anmihilation in the skin and cancerous systems. *Applied Suface Science*, 2008, **255**(1), 115.
12. Tak, Y., Hong, S. J., Lee, J. S. *et al.,* Fabrication of ZnO/CdScore/shell nanowire arrays for efficient solar energy conversion. *J. Matls.Chem.*, 2009, **19**(33), 5945.
13. Fan, H., Zhao, X., Yang, J. *et al.,* ZnO-graphene composite for photocatalytie degradation of methylene blue dye. *Catalysis Communications*, 2012, **29**, 29.
14. Chen Yingbo, Zhao Linfei, Wang Biao *et al.,* Structural growth process of zeolite imidazole skeleton material (ZIF-8). *J. Tianjin University of Technology,* 2016, **35**(5), 1.
15. Liu Ming-Ming, Lu Wen-Miao, Shi Xiu-Feng *et al.,* Characterization and catalytic properties of zeolite imidazolide framework materials (zif-8) synthesized by different methods. *Chinese J. Inorganic Chem.,* 2014, **30**(3), 579.
16. Hong Bao, Preparation and degradation of organic dyes by photocatalyst based on ZIF-8 complex. Master's degree thesis of Liaoning University, 2016: 28-37.
17. Liu Kefeng, Ren Dany, Sun Hui *et al.,* Synthesis of ZIF-8. Characterization and n-hexane adsorption performance. *Chinese J. C.*, 2016, **37**(10), 1856.
18. Liu Ming-Ming, Study on catalytic performance of zeolite imidazolide matrix material zif-8. Master's thesis of Taiyuan University of Technology, 2014: 29-39.
19. Zhang, L. J., Wei, Y. G., Wang, C.C. *et al.,* Hexatungstate subunit as building block in the hydrothermal synthesis of organic inorganic hybrid materials: synthesis, structure and optical properties of $CO_2$. *J. Solid State. Chem.,* 2004, **177**(10), 3433.
20. Wang Hui, Guo Xiaowei and Chen Guirong, Preparation of nano $CO_3O_4$ and photocatalytic properties by ball mill-assisted solid phase. *Chemical Research and Application*, 2016, **28**(12), 1744.
21 Zhao, C. Y., Shan, Q. J. and Wu, X F., Synthesis and photocatalytic properties of mesoporous structure Na10 [a-SiW,O34]/TiO2/Ag. *Chemical Research and Application*,2016 28(2), 154.
22. Zhou, J. W., Zhang, M. and Zhu, Y. F., Preparation of visible light driven g-C,N, @ ZnO hybrid photocatalyst *via* mechano-chemistry. *Phys. Chem.,Chemical Physics,* 2014, **16**(33), 17627.
23. Goo, J., Yang, J., Liu, Y. Y. *et al.,* Two novel 3D metal. organic frameworks based on two tetrahedral ligands: syntheses,structures, photoluminescence and photocatalytic properties. *Cryst. Eng. Comm.*, 2012, **14**. 6609.